Cancer Chemotherapy and Pharmacology (2019) 83:649–658
https://doi.org/10.1007/s00280-019-03770-0

ORIGINAL ARTICLE

Encapsulation of a new quinoxaline derivative in PLGA alters the pattern of its anticancer potency and induces apoptosis

Entsar A. Saad[1] · **Heba M. Waly**[1]

Received: 18 September 2018 / Accepted: 5 January 2019 / Published online: 16 January 2019

Abstract

Purpose Searching for novel anticancer therapeutics which are effective and primarily less toxic is urgently needed. Drug encapsulation provides more protection of drug within the body with more stable drug circulation levels thus avoiding drug peak-related adverse effects. We aimed first to develop and characterize a nano-particulate drug delivery system using poly(lactic-*co*-glycolic acid) (PLGA) for the new compound *N*-butylpyridoquinoxaline 1,4-dioxide (NBPQD), and second to investigate its anticancer effect and the probable mechanism.

Methods NBPQD–PLGA nano-particles were prepared and their shape, size, zeta potential, encapsulation efficiency (EE%), drug loading (DL%), drug release, anticancer activity against six human cancer cell lines, DNA binding ability, and flow cytometric analyses of apoptosis, cell cycle and caspase-3 activity were investigated.

Results and conclusions NBPQD–PLGA nano-particles were spherical with diameter around 54 nm. Zeta potential, EE%, and DL% values were − 20.4 mV, 88% and 21.8%, respectively. Nano-particles exhibited higher marked anticancer activities (much lower IC_{50}s) and changed the anticancer potency pattern towards all the studied cell lines compared to free NBPQD with superior potency against colorectal carcinoma (HCT-116, IC_{50} of 12.2 µg/mL). NBPQD–PLGA acts by induction of cancer cell apoptosis through oxidative stress, DNA damage, and activating a caspase-3 signaling pathway.

Keywords Quinoxaline · Cytotoxicity · DNA damage · Cell cycle · Caspase-3 · Anticancer

Introduction

Cancer is one of the leading causes of death worldwide [1–3]. It is characterized by proliferation of abnormal cells [4]. Surgery, chemotherapy, and radiotherapy are the standard methods used to treat cancer but they are usually of high cost and have serious adverse effects with restrictions of their use [5], thus there is an accelerated demand for efficient, less cost and more safe treatments with acceptable minimal or no adverse effects. Nano-particles (1–100 nm in size) can interact uniquely with bio-molecules and may aid in cancer treatment [6]. Many polymeric nano-carriers such as poly(lactic-*co*-glycolic acid) (PLGA) have been synthesized in the last few decades to act as delivery vehicles for chemotherapeutic medicines. It can significantly improve the anticancer efficiency of chemotherapeutic drugs [7] and increase patient satisfaction [8].

Quinoxaline (benzopyrazine) derivatives are a group of biologically active compounds containing pyrazoline ring system. They showed a wide spectrum of biological activities including antitumor, antioxidant, anti-inflammatory, antimicrobial, antidepressant, hypoglycemic, hypotensive, and antihistamic. Currently, there is a growing interest in their chemistry and their potential therapeutic applications. In particular, more concern has been directed to find quinoxaline-1,4-di-*N*-oxide derivatives with antitumor activity [9]. In this regard, we introduced *N*-butylpyridoquinoxaline 1,4-dioxide (NBPQD) as a newly synthesized quinoxaline derivative with remarkable antitumor activity against Ehrlich solid and liquid tumors [9, 10]. In the current study, we aimed to design and characterize biodegradable PLGA nano-particles loaded with NBPQD, and to investigate the anticancer activity of the newly designed NBPQD–PLGA nano-particles against free NBPQD. Investigation of the probable mechanism of action was also intended.

✉ Entsar A. Saad
entsarsaad@gmail.com

[1] Chemistry Department, Faculty of Science, Damietta University, Damietta 34517, Egypt

Human tumor cell lines including hepatocellular carcinoma (HepG2), mammary gland (MCF-7), colorectal carcinoma (HCT-116), epithelioid carcinoma (Hela), human prostate cancer (PC3) and epidermoid carcinoma (Hep2) cancer cells were used as in vitro cancer models.

Materials and methods

Cell lines and chemicals

Human cell lines were obtained via holding company for biological products and vaccines (VACSERA, Cairo, Egypt). PLGA (lactide/glycolide ratio of 50:50, carboxylic acid end group, molecular weight, 17 kDa) and polyvinyl alcohol (PVA) 80% hydrolyzed were purchased from Sigma-Aldrich, China. RPMI-1640 medium, MTT, and DMSO were purchased from Sigma, St. Louis, USA. Fetal bovine serum was bought from GIBCO, UK. All other chemicals were of analytical grade.

Preparation and characterization of NBPQD

Quinoxaline derivative, NBPQD (Fig. 1), was synthesized, characterized and kindly provided by Prof. M.A. Waly, Chemistry Department, Faculty of Science, Damietta University, Egypt. It was synthesized via utilization of an active allylic methyl group. NBPQD product was purified via column chromatography using 2% ethanol/dichloromethane as eluent. NBPQD ($C_{15}H_{15}N_3O_3$) melting point is 225–226 °C. It is hardly soluble in water but easily soluble in DMSO. IR spectra ($\bar{\upsilon}$ = 1670 (CO), 1612 (C=C), 1340 (N–O) cm^{-1}) displayed absorption for the new cyclized amide carbonyl group at 1670 cm^{-1}. ^{1}H NMR data ($\delta = 1.00$ (3H, t, $J = 7.3$ Hz, CH_3), 1.45 (2H, m, CH_3CH_2), 1.82 (2H, quint, $CH_2CH_2CH_2$), 4.10 (2H, t, $J = 7.3$ Hz, CH_2N), 7.27–7.29 (2H, m, H-6 and H-7), 7.84–7.87 (2H, m, H-5 and H-8), 8.43 (1H, d, $J = 9.3$ Hz, H_b), 8.62 (1H, d, $J = 9.3$ Hz, H_a) ppm reflected downfield shifting for the H_b proton to the aromatic proton region. ^{13}C NMR data: $\delta = 13.84$, 20.00, 31.14, 50.01, 116.75, 120.11, 131.89, 137.94, 138.55, 140.45, 144.54, 146.48, 147.37, and 160.16 ppm. The coupling constant J is around 9.3 Hz reflecting its existence in cis form. UV data did not show a significant red shifting ($\lambda_{max} = 261$–274 nm). MS data: m/z (%) = 269 (M^+–O, 42.4), 253 (M^+–2O, 41.2), 212 ($C_{11}H_6N_3O_2$, 20.0), 184 ($C_{10}H_6N_3O$, 14.1), 168 ($C_{10}H_6N_3$, 34.1), 141 ($C_9H_5N_2$, 41.2), and 128 ($C_8H_4N_2$, 11.8).

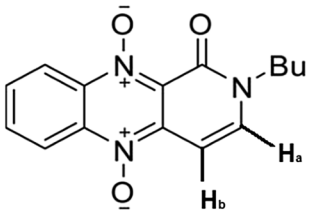

Fig. 1 Chemical structure of *N*-butylpyridoquinoxaline 1,4-dioxide (NBPQD)

Preparation of NBPQD nano-particles

NBPQD nano-form in PLGA was prepared via emulsion technique. This technique is based on the formation of oil-in-water emulsion via two PLGA solutions. Solution 1 is oil phase where 50 mg of PLGA 50:50 (17 kDa) and a desired amount of the drug (10 mg) were dissolved in 3 mL chloroform, and solution 2 is water phase composed of 20 mL 4% aqueous PVA (80% hydrolyzed) as a surfactant. Polymeric beads are obtained when oil phase solution is added to water phase solution dropwise [11]. Oil-in-water emulsion solution was then stirred for 24 h using magnetic stirrer. Thereafter, the resultant nano-particles were lyophilized. Solid NBPQD–PLGA particles can be stored up to 3 months or up to 3–4 days at 4 °C if solubilized in water. Nano-particle solution was freshly prepared for every use.

Characterization of NBPQD–PLGA nano-particles

Morphology and particle size

NBPQD–PLGA particles' shape and size were examined via high-resolution transmission electron microscopy (TEM). On an amorphous carbon-coated copper grid, one drop from a highly diluted sample solution was deposited and air-dried. Imaging was achieved using a Joel JEM-2100 microscope; accelerating voltage 200 kV with Gatan Erlangshen ES500 digital camera.

Particle zeta potential

A nano-ZetaSizer apparatus (Malvern Instruments, UK) was used to determine the zeta potential of NPBQD–PLGA nano-particles. The zeta potential was determined by electrophoretic light scattering studies performed in an aqueous solution and Smoluchowski software approximation was used to calculate the zeta potentials. The measurements were recorded at 25 °C and started after 2 min to allow the temperature to equilibrate.

NBPQD encapsulation efficiency (EE%) and drug loading (DL%)

NBPQD amount encapsulated in PLGA nano-particles was calculated by subtracting non-encapsulated NBPQD amount

in the supernatant of the nano-particle suspension removed after centrifugation, measured using fluorescence spectrometry at $\lambda = 275$ nm, from initial NBPQD quantity used for nano-particle preparation. Non-encapsulated NBPQD level was estimated via a standard curve. EE% and DL% were calculated using the following equations:

$$\text{EE}\,(\%) = (\text{amount of NBPQD in nano-particles}/\text{initial amount of NBPQD used for encapsulation}) \times 100;$$

$$\text{Drug loading}\,(\%) = (\text{actual weight of drug in nano-particles}/\text{weight of nano-particles}) \times 100.$$

In vitro drug release study

In vitro release of NBPQD from PLGA nano-particles was evaluated using dialysis bag diffusion technique after the preparation of NBPQD–PLGA nano-particles as described previously with minor modifications [12]. Briefly, 10 mg of NBPQD–PLGA nano-particles were suspended in 1 mL of 0.1 M phosphate-buffered saline (PBS, pH 7.4). The solution was placed in a pre-swelled dialysis bag with 4 kDa molecular weight cut-off (Sigma) and immersed in 20 mL of 0.1 M PBS, pH 7.4, at 37 °C with gentle agitation. At different times, 1 mL of incubation medium was analyzed to measure NBPQD concentration as described above. The incubation medium was immediately supplemented with a new 1 mL of fresh PBS to maintain the volume. The concentration of NBPQD released from nano-particles was expressed as a percentage of total NBPQD in the nano-particles and plotted as a function of time.

Cytotoxicity assay

MTT colorimetric assay was used to estimate NBPQD and NBPQD–PLGA inhibitory effects on cell growth (proliferation). In viable cells, yellow tetrazolium bromide (MTT) is converted into purple formazan derivative in the presence of mitochondrial succinate dehydrogenase. In 5% CO_2 incubator, cell lines were cultured in RPMI-1640 medium with 10% fetal bovine serum in the presence of 100 units/mL penicillin and 100 µg/mL streptomycin at 37 °C. Cell lines were implanted in a 96-well plate (1×10^4 cells/well) at 37 °C for 48 h. Then cells were treated with different concentrations of tested compounds and incubated for 24 h. After this, 20 µL of MTT solution (5 mg/mL) was added and incubated for 4 h. 100 µL of DMSO were added to each well to dissolve the obtained purple formazan, the absorbance (A) was read at 570 nm using a plate reader (EXL 800, USA) and the relative cell viability percent was determined (A_{570} of treated sample/A_{570} of untreated sample) × 100 [13].

Methyl green assay

Methyl green reversibly binds polymerized DNA, and the complex is stable at neutral pH, whereas free methyl green fades. Incubation in the buffer used for displacement reactions for 24 h results in virtually complete loss of methyl green absorbance. A colorimetric assay was used to measure the displacement of methyl green from DNA by compounds with the ability to bind to DNA. The displacement was determined spectrophotometrically via the decrease in absorbance at 630 nm [14].

Cell cycle analysis

HCT-116 cells were seeded into six-well plates. The cells were treated with IC_{50} concentration of NBPQD, NBPQD–PLGA, and PLGA (the equivalent amount of PLGA in NBPQD–PLGA) for 24 h. After being washed twice with PBS, cells were harvested and collected by centrifugation at 350 g for 5 min, fixed with 70% ethanol, and then stored at − 20 °C overnight. Next, cells were collected by centrifugation and stained by 100 µL propidium iodide (PI) staining solution (5 µg/mL RNase and 20 µg/mL PI) at room temperature for 30 min avoiding light, followed by analysis with flow cytometer (Becton Dickinson, Sunnyvale, CA, USA).

Caspase-3 activity

HCT-116 cells were left untreated (control) or treated with IC_{50} concentration of NBPQD, NBPQD–PLGA, and PLGA (the equivalent amount of PLGA in NBPQD–PLGA) for 24 h to induce apoptosis. Cells that were washed in PBS were fixed and permeabilized using BD Cytoperm™ Kit for 20 min at room temperature, pelleted, washed with BD Perm/ Wash TM buffer, and stained with FITC rabbit anti-active caspase-3 antibody. Stained cells were then washed and resuspended in BD Perm/Wash™ buffer before analyzing by flow cytometry.

Apoptosis analysis

Cell apoptosis was determined using Annexin V-FITC/PI apoptosis detection kit according to the manufacturer's instructions (Beyotime, China). Briefly, after treatment with fresh medium or with IC_{50} concentration of NBPQD, NBPQD–PLGA, and PLGA (the equivalent amount of PLGA in NBPQD–PLGA) for 24 h, HCT-116 cells were washed with cold PBS and suspended in 500 µL of Annexin V binding buffer. After incubation with 5 µL of FITC-labeled Annexin V and 5 µL of PI for 30 min at room temperature in

the dark, cell samples were immediately analyzed using flow cytometer as previously described [15].

Statistical analysis

Data are introduced as mean ± SD; $n = 3–5$ separate determinations. Student's t test was used for comparison between two groups and $P < 0.05$ was considered significant. Statistical analyses were done using instat version 2.03 (Graphpad, USA).

Results and discussion

Most chemotherapeutic drugs have fast blood clearance, low tumor selectivity, and high toxicity towards normal cells/tissues. This limits their further clinical application in cancer treatment purposes. Using nano-particles may decline chemotherapeutic drug side effects, improve their distribution in the body, increase their specificity, prolong activity, and improve their in vivo degradation resistance [16]. Previously, we reported NBPQD as active antitumor agent [9, 10]. Therefore, development of an effective nano-delivery system in a trial to improve NBPQD chemotherapeutic efficacy towards cancer was intended.

The present study is an attempt to encapsulate and deliver the NBPQD to the cancer site using emulsification technique. PLGA was chosen for its reported attractive characteristics including excellent biocompatibility and biodegradability. PLGA nano-drug delivery system ensures aqueous solubility of hydrophobic drugs and maintains drug release at its target cells [17].

Characterization of NBPQD–PLGA nano-particles

Morphology and particle size

Nano-particle size < 500 nm is acceptable for intravenous injection [8]. As evidenced in Fig. 2, TEM images showed that the prepared NBPQD–PLGA nano-particles are spherical in shape with a mean diameter of 54 nm (54 ± 8 nm) suggesting availability for its intravenous use. Small nano-particle size here also propose passive tumor targeting through enhanced permeability and retention (EPR) effect with reduction of drug delivery to normal (non-target) tissues. This is in the same line with Lee et al. [18] who stated that nano-particle bio-distribution is decided by their size; nano-particles < 5 nm are quickly filtered out by the kidneys but nano-particles > 200 nm accumulate within the spleen, liver, and lung. Nano-particles are incapable to go out from the intravascular space in normal tissues, restricting their volume of distribution, while they are capable to readily exit leaky tumor-associated vessels. This EPR effect, therefore, passively targets tumors but limiting drug delivery to non-target tissues. Accordingly, to avoid clearance by the reticuloendothelial system of macrophages within the liver and spleen while still being able to take advantage of EPR effect, nano-particles should have sizes under 200 nm.

Particle zeta potential

Zeta potential value is indicative of colloidal stability. High positive or negative zeta potential values are preferable to guarantee high stability against particle aggregation. Heydari and Rashidipour (2015) [19] stated that nano-particles with values > + 25 or < − 25 mV are highly stable. Zeta potential of the newly synthesized NBPQD–PLGA

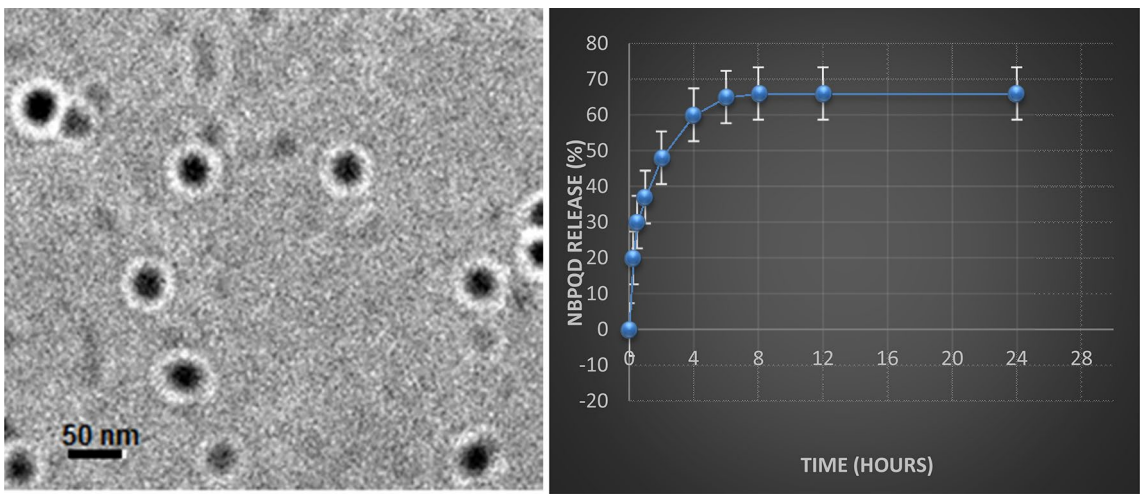

Fig. 2 Transmission electron micrograph of NBPQD–PLGA nano-particles and in vitro profile of NBPQD release from PLGA in phosphate-buffered saline (PBS, pH 7.4). Results are presented as mean ± SD; $n = 3–5$ separate determinations

nano-particles equals -20.4 ± 7.04 mV indicating that the system is physically stable as the high negative charge can cause strong repulsive force among particles, which prevent particle aggregation.

NBPQD encapsulation efficiency (EE%) and drug loading (DL%)

Depending on the prepared size of the administered drug (micro or nano), the drug dosage varies. Besides, the recommended dose of nano-size varies in turn depending on the formulation of the drug [20]. Encapsulation efficiency and actual drug loading for NBPQD in PLGA were 88% and $21.8 \pm 0.25\%$, respectively, indicating high incorporation of NBPQD into PLGA nano-particles. This high EE% is expected to directly improve the efficiency of drug administration; it would contribute in reductions of both drug administration frequency and treatment duration. Thus, encapsulation of NBPQD in PLGA could be important for enhancing the drug bioavailability. Dias et al. (2015) [8] and other researchers also reported high drug encapsulation efficiency using PLGA drug delivery system to hydrophobic drugs. This behavior is attributed to the organic medium where encapsulation process is achieved. High drug loading capacity of delivery system has clinical relevance.

Drug release study

In vitro release of NBPQD from PLGA nano-particles was studied for 24 h. Drug release from PLGA nano-particles usually occurs in a biphasic manner, with an initial burst phase followed by sustained release. In the current study, an initial burst phase corresponding to about 30–35% was observed within 1 h due to the drug desorption and release from nano-particle surface. A sustained NBPQD release to a total of about 65–70% was found for the nano-particle over the entire period of study as shown in Fig. 2. It means that most of the drug was incorporated inside PLGA nano-particles. For delivery of anticancer drugs, the initial burst release is critical for quick drug delivery to reach sufficient initial quantity that can murder cancer cells and the sustained release is as well crucial to inhibit further proliferation and migration for cancer cells that may stay alive from the initial burst [21].

NBPQD–PLGA nano-particles anticancer effect and the possible mechanisms of action

Cytotoxicity and cancer cell proliferation

The in vitro study represents an ideal model for human disease investigation as it has a high degree of transparency and ability to find out the drug concentration for in vivo experiments. In the present study, different human cancer cells were treated with different concentrations of NBPQD, PLGA and NBPQD–PLGA ranging from 0.0 (control) to 100 µg/mL. As expected, free NBPQD displayed different degrees of dose-dependent cytotoxicity against different human cell lines (Fig. 3) confirming our previous conclusion about free NBPQD as a new active antitumor agent [9, 10]. This NBPQD anti-proliferative activity could be related to the activation of 1,4-dioxide moiety to cytotoxic free radical. This free radical, like others, has the ability to generate chain reactions when bound to cellular biological molecules [22, 23], which are lethal to the cell [24–29] leading to cellular proliferation suppression and ultimately cell death. Other investigations presented other quinoxaline 1,4-di-*N*-oxide derivatives that showed selective cytotoxicity against hypoxic cells present in solid tumors [9]. Quinoxaline 1,4-dioxides were believed to act through the creation of a free radical intermediate generated by single electron transfer from the electron-rich medium to the electron-poor N centers of 1,4-di-*N*-oxide moiety [30].

NBPQD–PLGA showed more pronounced cytotoxicities against all types of the studied human cancer cells than free NBPQD (IC_{50} ranged from 12.2 to 32.7 µg/mL for NBPQD–PLGA versus IC_{50} ranged from 33.7 to 65.4 µg/mL for free NBPQD) (Table 1). In more detail, NBPQD–PLGA exhibited strong anti-proliferation efficacy against human HCT-116, Hep2 and Hela cells with IC_{50} of 12.2, 16.5 and 20.4 µg/mL, respectively, while the cytotoxic effect of free NBPQD on human HCT-116 and Hep2 cells was moderate with IC_{50} of 42 and 38 µg/mL, respectively, and was weak on human Hela cells with IC_{50} of 65.4 µg/mL. Nano-particles have the tendency for adsorption onto cell membrane resulting in a gradient that favors drug entrance into the cell. Upon this, increased cytotoxic effect of NBPQD–PLGA delivery system was expected because of efficient cellular uptake of nano-particles via endocytosis. This was in great harmony with Borah et al. [17]. It must be mentioned that PLGA has almost negligible effect on cancer cells viability (Fig. 3). This suggests that the observed therapeutic anti-proliferative efficacy is only attributed to the loaded drug (NBPQD) within PLGA nano-particles. Nevertheless, it is worthy to state that the observed anticancer activity of free NBPQD was most potent against MCF-7 followed by Hep2, HCT-116, PC3, HepG2 then Hela but when encapsulated in PLGA the observed pattern of anticancer potency was changed to be in the following order: HCT-116, Hep2, Hela, MCF-7, HepG2 and PC3. This may be explained on the basis of differences in both rate and extent of PLGA nano-particle cellular uptake by different human cell lines. These results indicate that utilization of NBPQD–PLGA delivery system not only enhances NBPQD anticancer efficacy against all the studied cell lines, evidenced by reduction in IC_{50} values for all, but also can change NBPQD anticancer responsiveness

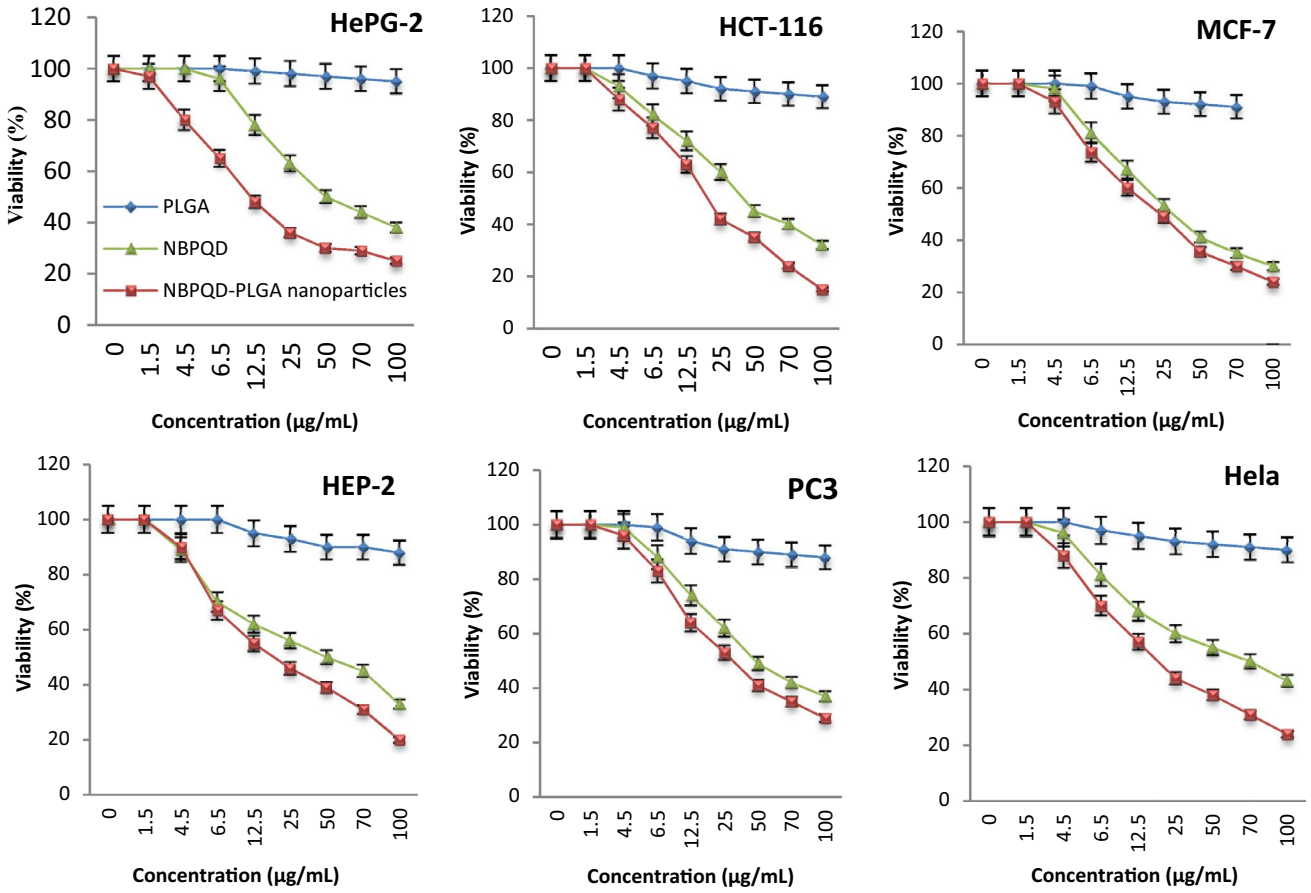

Fig. 3 Effects of free PLGA, free NBPQD and NBPQD–PLGA nanoparticles on cell proliferation (relative viability %) of the studied human tumor cells. Results are presented as mean ± SD; $n = 3$–5 separate determinations. Cells were treated with different concentrations of tested compounds for 24 h

Table 1 IC_{50} of PLGA, NBPQD, and NBPQD–PLGA for the studied human tumor cells

Compounds	In vitro cytotoxicity IC_{50} (µg/mL)[a]					
	HepG2	HCT-116	MCF-7	PC3	Hep2	Hela
NBPQD-PLGA	27.1 ± 2.04***	12.2 ± 0.97***	24.3 ± 1.87***	32.7 ± 2.43***	16.5 ± 1.14***	20.4 ± 1.35***
NBPQD	52.9 ± 3.82	42.0 ± 3.14	33.7 ± 2.82	49.0 ± 3.69	38.0 ± 2.71	65.4 ± 3.95
PLGA	> 100 ± 3.5	> 100 ± 2.8	> 100 ± 4.1	> 100 ± 3.3	> 100 ± 4.15	> 100 ± 3.6

Results are presented as mean ± SD; $n = 3$–5 separate determinations. Tumor cells were treated with different concentrations of tested compounds for 24 h. IC_{50} is the concentration that caused 50% cell growth inhibition.

***$P < 0.001$ versus NBPQD

[a]1–10 is very strong, 11–20 is strong, 21–50 is moderate, 51–100 is weak, and > 100 is non-cytotoxic

pattern towards different types of cancers, as obviously evidenced by changed cancer cell line order based on the degree of anticancer response.

DNA binding

It was evidenced that quinoxaline antibiotics are suppressors of DNA synthesis [29]. Moreover, DNA damage was postulated as the mechanism of action of quinoxaline derivatives and it was established for 7-chloro-3-[[(*N*,*N*-dimethyl-amino)propyl]amino]-2-quinoxaline carbonitrile 1,4-di-*N*-oxide hydrochloride in colorectal adenocarcinoma (Caco-2) cells under hypoxic and well-oxygenated conditions by Azqueta et al. [32].

To explore the possible mechanisms behind the revealed cell growth suppression by our compound, methyl green

assay was done. Obtained results in Table 2 were supportive to the suggestion that both NBPQD and NBPQD–PLGA have anti-proliferation activity. Both displayed abilities to bind DNA resulting in DNA damage, DNA synthesis arrest and ultimately cell killing via inducing apoptosis. As expected, NBPQD–PLGA ability was more superior than free NBPQD evidenced by lower IC_{50}. These results are actually in harmony with Azqueta et al. [32], Frankfurt and Krishan (2003) [33], Elsayed et al. (2018) [34] who stated that induction of tumor cell apoptosis is a crucial mechanism for an anticancer compound, and Feng et al. (2018) [35] who stated ''nano-particles can suppress cell viability by different mechanisms such as apoptosis and free radicals release''.

Cell cycle alterations

Since the degree or progression of apoptosis in a cell population can be measured by quantifying the ratio of cells in sub-G1 in relation to the other phases [36], the effects on cell cycle phases on HCT-116 cells, the most susceptible cell line in the cytotoxicity test, were flow cytometrically tested. As illustrated in Table 3, the population of G1 declined as the population of sub-G1 cells increased. Increase in cells entering the sub-G1 phase from 5.7 ± 0.45% in untreated cancer cells (control) to 17.96 ± 0.2% in cancer cells exposed to free NBPQD and to 20.4 ± 0.2% ($P < 0.001$) in those exposed to NBPQD–PLGA indicates more cell apoptosis obviously associated more with nano-form. Apoptotic cells undergo DNA fragmentation; fragmented DNA separates out from apoptotic cells when hydrated during DNA staining and apoptotic cells finish up with nearly 20–50% DNA of that of G1 cells, developing a distinctive sub-G1 peak. On the other hand, in S phase, it can be seen that the percentage of cells was also increased at the expense of G2/M peak (8.5 ± 0.15% for free NBPQD and 10.96 ± 0.2% for nano-form) compared to the control (5.4 ± 0.15%, $P < 0.001$) indicating that our compound delays cell cycle progression at S phase. Advancement through the S phase is regulated by the observation of replication checkpoints and avoiding excessive DNA synthesis. In the case of DNA damage, G1/S checkpoint inhibits cell cycle progress [37]. Hence, it is possible that the increment of cells in S phase was due to the incorporation of free NBPQD/NBPQD–PLGA nano-particles into DNA during the process of DNA replication.

Based on the above results, it can be stated that both free NBPQD and NBPQD–PLGA nano-particles inhibit cancer cell growth mainly via the induction of apoptosis; however, nano-form is more potent. These results are in agreement with our aforementioned cell viability data and verify the potency of the prepared PLGA nano-particles in delivering drugs to the cells.

Table 2 DNA/methyl green colorimetric assay of NBPQD and NBPQD–PLGA

DNA-active compound	IC_{50} (μg/mL)
BPQD–PLGA	$46.2 \pm 2.8^{!!}$
NBPQD	52.8 ± 3.1

Results are presented as mean ± SD; $n = 5$ separate determinations. IC_{50} is the concentration required for a 50% decrease in the initial absorbance of the DNA/methyl green solution

$^{!!}P < 0.01$ versus NBPQD

Apoptosis analysis

Annexin V/PI-based flow cytometry was applied to introduce further evidence for NBPQD-induced cancer cell death. Table 4 shows that the proportion of cell death (late apoptotic) was greater ($P < 0.0001$) in cells treated with NBPQD–PLGA (10.75%) compared with those treated with free NBPQD (3.05%) or with the proportion of cell death of PLGA (0.91%) and control HCT-116 cell line (0.49%) indicating that nano-particles are associated with more apoptotic cell death. This high apoptotic induction may be attributed to their higher affinity towards DNA binding as evidenced via methyl green assay and explains their more pronounced cytotoxic effect on cancer cells presented above. This is in harmony with [38] which reported that the nano-particle delivery system enhances cell death.

Table 3 Cell cycle progression and activity of caspase-3 of HCT-116 cells after treatments with IC_{50} of NBPQD and NBPQD–PLGA nano-particles for 24 h

Compounds	Cell cycle progression (%)				Caspase-3 activity (%)
	Sub-G1	G0/1	S phase	G2/M	
HCT-116 (control)	5.7 ± 0.45	74.5 ± 0.3	5.4 ± 0.15	6.36 ± 0.15	21.6 ± 0.55
PLGA	6.5 ± 0.15	73.16 ± 0.76	6.0 ± 0.3	5.8 ± 0.2	22.8 ± 0.11
NBPQD	$17.96 \pm 0.2^{\#}$	67.2 ± 0.55*	$8.5 \pm 0.15^{\#}$	$3.2 \pm 0.2^{\#}$	30 ± 0.11*
NBPQD-PLGA	$20.4 \pm 0.2^{\#, ***}$	$57.13 \pm 0.56^{\#, !!!}$	$10.96 \pm 0.2^{\#, ***}$	$1.66 \pm 0.15^{\#, ***}$	$39.6 \pm 0.53^{\#, ***}$

Results are presented as mean ± SD; $n = 3$ separate determinations

$^{\#}P < 0.0001$ and $^{*}P < 0.001$ versus HCT-116 control cells, $^{***}P < 0.001$ and $^{!!!}P < 0.0001$ versus NBPQD

Table 4 Annexin V/PI- based apoptosis analysis on HCT-116 cancer cells after treatments with IC_{50} of NBPQD and NBPQD–PLGA nano-particles for 24 h

Compounds	Late apoptosis (%)	Necrosis (%)	Early apoptosis (%)	Viable cells (%)
HCT-116 (control)	0.49 ± 0.14	0.32 ± 0.03	0.34 ± 0.02	98.8 ± 0.1
PLGA	0.91 ± 0.14	0.39 ± 0.014	0.52 ± 0.02	98.3 ± 0.15
NBPQD	$3.05 \pm 0.07^{!}$	$13.45 \pm 0.07^{\#}$	$0.56 \pm 0.01^{!!}$	$82.7 \pm 0.25^{\#}$
NBPQD–PLGA	$10.75 \pm 0.21^{\#,!!!}$	$15.75 \pm 0.07^{\#,!!!}$	$0.54 \pm 0.03^{!!}$	$72.9 \pm 0.36^{\#,!!!}$

Results are presented as mean ± SD; $n = 3$ separate determinations

$^{\#}P < 0.0001$ and $^{!}P < 0.01$ versus HCT-116 control cells, $^{!!!}P < 0.0001$ and $^{!!}P < 0.01$ versus NBPQD

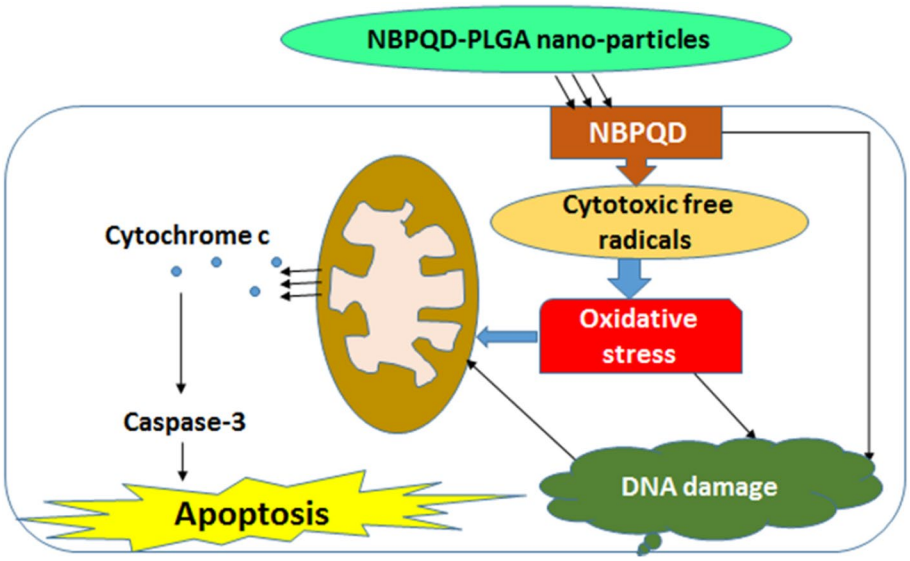

Fig. 4 Proposed mechanism of action of NBPQD–PLGA. Adsorbed NBPQD–PLGA nano-particles onto cell membrane result in a gradient that favors drug (NBPQD) entrance into the cell. Inside cancer cell, DNA is damaged either by DNA–drug binding or through the drug generation of cytotoxic free radicals that causes peroxidation of lipids, protein and DNA. Oxidative stress/DNA damage triggers apoptotic intrinsic mitochondrial pathway in which cytochrome c leaks from the mitochondrial membrane to the cytosol resulting in caspase-3 activation that initiates cell apoptosis events

Caspase-3 activity

Caspase-3 activation is well reported to be essential for inducing apoptosis. Compounds with a quinoxaline ring in their structure have the ability to inhibit the angiogenic process and to induce caspase-dependent apoptotic cell death. Other further anti-proliferative mode of actions such as free radical release adds more support to the idea that quinoxalines could be prospective applicants for the management of cancer [39].

Flow cytometry analysis in Table 3 showed that caspase-3 activation was induced by either free NBPQD or NBPQD–PLGA nano-particles in HCT-116 cancer cells. Free PLGA did not affect the caspase-3 activity in comparison with negative control. It was also obvious that NBPQD–PLGA nano-particles accelerated caspase-3 activity more than free NBPQD ($P < 0.001$). Thus, it can be suggested that NBPQD–PLGA nano-particles induce apoptosis in cancer cells through activating a caspase-3 signaling pathway (Fig. 4). Our study results are in line with those of other researchers concluding that compared to free drug, nano-particle–drug conjugates stimulate stronger activation of apoptosis signaling pathways [38, 40].

In conclusion, results of the present study revealed that targeting cancer cells with NBPQD–PLGA nano-particles rather than free NBPQD results in much better toxicity and enhances more apoptotic tumor cell death. These results indicate that utilization of NBPQD–PLGA delivery system not only improves NBPQD anticancer efficacy but also alters its anticancer potency pattern. NBPQD either in its free or nano-form induces cancer cell apoptosis through the activation of a caspase-3 signaling pathway. NBPQD–PLGA nano-particles as a new potential anticancer therapeutic deserve a chance to be tested more for more validation.

Acknowledgements Authors would like to thank Prof. Salem A. Habib and Prof. Mohamed A. Waly, Chemistry Department, Faculty of Science, Damietta University, Egypt, for their valuable help.

Funding None.

Compliance with ethical standards

Conflict of interest Author Entsar A. Saad declares that she has no conflict of interest. Author Heba M. Waly declares that she has no conflict of interest.

Ethical approval This article does not contain any studies with human participants or animals performed by any of the authors.

References

1. El-Emshaty HM, Saad EA, Gouida MS, Elshahawy ZR (2018) Associations between CD133, CK19 and G2/M in cirrhotic HCV (genotype-4) patients with or without accompanying tumor. Biocell 42(2):55–60
2. Attallah A, El-Far M, Abdel Malak C, Omran M, Farid K, Yahya R et al (2015) A simple diagnostic index comprising epithelial membrane antigen and fibronectin for hepatocellular carcinoma. Ann Hepatol 14:869–880
3. Saad EA, Hassanien MM, Elneely EA (2017) Iron(III) diacetylmonoxime–2-hydrazinopyridine complex: a new prospective antitumor drug. Appl Organometal Chem 31(9):e3684. https://doi.org/10.1002/aoc.3684
4. Saad EA, Hassanien MM, El-Lban FW (2017) Nickel(II) diacetyl monoxime-2-pyridyl hydrazone complex can inhibit Ehrlich solid tumor growth in mice: a potential new antitumor drug. Biochem Biophys Res Commun 484:579–585. https://doi.org/10.1016/j.bbrc.2017.01.137
5. Saad EA, Hassanien MM, El-Mezayen H, ELmenawy NM (2017) Regression of murine Ehrlich ascites carcinoma using synthesized cobalt complex. MedChemComm 8:1103–1111. https://doi.org/10.1039/C6MD00618C
6. Nagajyothi PC, Muthuraman P, Sreekanth TVM, Kim DH, Shim J (2017) Green synthesis: in-vitro anticancer activity of copper oxide nanoparticles against human cervical carcinoma cells. Arabian J Chem 10:215–225
7. Wang H, Zhao Y, Wu Y, Hu Y, Nan K, Nie G et al (2011) Enhanced anti-tumor efficacy by co-delivery of doxorubicin and paclitaxel with amphiphilic methoxy PEG-PLGA copolymer nanoparticles. Biomaterials 32:8281–8290
8. Dias DJS, Joanitti GA, Azevedo RB, Silva LP, Lunardi CN, Gomes AJ (2015) Chlorambucil encapsulation into PLGA nanoparticles and cytotoxic effects in breast cancer cell. J Biophysical Chem 6:1–13
9. Al-Mutairi FM, Abdel-Daim MM, Ibrahim IT, Habib SA, Waly HM (2016) The potent effect of a newly synthesized *N*-Butylpyridoquinoxaline 1,4-dioxide (NBPQD) derivative as antitumor agent in solid tumor model. Int J Pharm Res Allied Sci 5:203–218
10. Habib SA, Ibrahim IT, Abd-Eldaye MA, El-Sheshtawey MM, Waly HM (2012) *N*-Butylpyridoquinoxaline 1,4-dioxide (NBPQD) as a new potent for tumor imaging and therapy. Nat Sci 4:1074–1084
11. Homan KA, Chen J, Schiano A, Mohamed M, Willets KA, Murugesan S et al (2011) Silver–polymer composite stars: synthesis and applications. Adv Funct Mater 21:1673–1680
12. Li XL, Li RT, Qian X, Ding Y, Tu Y, Guo R, Hu Y et al (2008) Superior antitumor efficiency of cisplatin-loaded nanoparticles by intratumoral delivery with decreased tumor metabolism rate. Eur J Pharm Biopharm 70:726–734
13. Mauceri HJ, Hanna NN, Beckett MA, Gorski DH, Staba MJ, Stellato KA et al (1998) Combined effects of angiostatin and ionizing radiation in antitumour therapy. Nature 349:287–291
14. Burres NS, Frigo A, Rasmussen RR, McAlpine JB (1992) A colorimetric microassay for the detection of agents that interact with DNA. J Nat Prod 55:1582–1587
15. Jin H, Pi J, Yang F, Jiang J, Wang X, Bai H et al (2016) Folate-chitosan nanoparticles loaded with ursolic acid confer anti-breast cancer activities in vitro and in vivo. Sci Rep 6:30782. https://doi.org/10.1038/srep30782
16. Chuan L, Jia Z, Yu-Jiao Z, Shu-Fang N, Jun C, Qian W et al (2015) Biocompatible and biodegradable nanoparticles for enhancement of anti-cancer activities of phytochemicals. Chin J Nat Med 13:641–652
17. Borah A, Palaninathan V, Girija AR, Balasubramanian S, Rochani AK, Maekawa T (2017) Poly-lactic-*co*-glycolic acid nanoformulation of small molecule antagonist GANT61 for cancer annihilation by modulating hedgehog pathway. NanoWorld J 3:1–10
18. Lee MS, Dees EC, Wang AZ (2017) Nanoparticle-delivered chemotherapy: old drugs in new packages. Oncology J 31:198–208
19. Heydari R, Rashidipour M (2015) Green synthesis of silver nanoparticles using extract of Oak fruit hull (jaft): synthesis and in vitro cytotoxic effect on MCF-7 cells. Int J Breast Cancer 846743:1–6
20. Ong SGM, Ming LC, Lee KS, Yuen KH (2016) Influence of the encapsulation efficiency and size of liposome on the oral bioavailability of griseofulvin-loaded liposomes. Pharmaceutics 8(3):25. https://doi.org/10.3390/pharmaceutics8030025
21. Liu D-q, Cheng Z-q, Feng Q-j, Li H-j, Ye S-f, Teng B (2018) Polycaprolactone nanofibres loaded with 20(*S*)-protopanaxadiol for in vitro and in vivo anti-tumour activity study. R Soc Open Sci 5(5):180137. https://doi.org/10.1098/rsos.180137
22. Saad EA, El-Gayar HA, El-Demerdash RS, Radwan KH (2018) Hepato-toxic risk of gum arabic during adenine-induced renal toxicity prevention. J Appl Pharm Sci 8(12):104–111. https://doi.org/10.7324/JAPS.2018.8801
23. Saad EA, El-Gayar HA, El-Demerdash RS, Radwan KH (2018) Frankincense administration antagonizes adenine induced chronic renal failure in rats. Phcog Mag 14(58):634–640. https://doi.org/10.4103/pm.pm_271_18
24. Habib SA, Saad EA, Elsharkawy AA, Attia ZR (2015) Pro-inflammatory adipocytokines, oxidative stress, insulin, Zn and Cu: Interrelations with obesity in Egyptian non-diabetic obese children and adolescents. Adv Med Sci 60:179–185
25. Saad EA, Habib SA, Refai WA, Elfayoumy AA (2017) Malondialdehyde, adiponectin, nitric oxide, C-reactive protein, tumor necrosis factor-alpha and insulin resistance relationships and interrelationships in type 2 diabetes early stage. Is metformin alone adequate in this stage? Int J Pharm Pharm Sci 9(10):176–181. https://doi.org/10.22159/ijpps.2017v9i10.21149
26. Saad EA, Hassanien MM, El-Hagrasy MA, Radwan KH (2015) Antidiabetic, hypolipidemic and antioxidant activities and protective effects of *Punica granatum* peels powder against pancreatic and hepatic tissues injuries in streptozotocin induced IDDM in rats. Int J Pharm Pharm Sci 7(7):397–402. https://innovareacademics.in/journals/index.php/ijpps/article/view/6705/2649
27. Saad EA, Toson EA, Ahmed GM (2015) Clove or green tea administration antagonizes khat hepatotoxicity in rats. Int J Pharm Pharm Sci 7(6):72–76
28. Saad EA, Habib SA (2013) Effect of crude extracts of some medicinal plants on the osmotic stability of human erythrocytes in vitro. J Free Rad Antioxidants Photon 139:265–272. https://sites.google.com/site/photonfoundationorganization/home/the-journal-of-freeradicals-and-antioxidants
29. Toson EA, Habib SA, Saad EA, Harraz NH (2014) Toxic and antifertility effects of *Alocasia macrorrhiza* and *Calotropis procera* ethanolic extracts on male mice. Int J Biochem Photon 195:328–338. https://sites.google.com/site/photonfoundationorganization/home/internationaljournal
30. Priyadarsini KI, Dennis MF, Naylor MA, Stratford MRL, Wardman P (1996) Free radical intermediates in the reduction of quinoxaline *N*-oxide antitumor drugs: redox and prototropic reactions. J Am Chem Soc 118:5648–5654
31. Xu Y, McSally J, Andricioaei I, Al-Hashimi HM (2018) Modulation of Hoogsteen dynamics on DNA recognition. Nature Comm

9:Article number: 1473. https://doi.org/10.1038/s41467-018-03516-1
32. Azqueta A, Pachon G, Cascante M, Creppy EE, Lopez de Cerain A (2005) DNA damage induced by a quinoxaline 1,4-di-*N*-oxide derivative (hypoxic selective agent) in Caco-2 cells evaluated by the comet assay. Mutagenesis 20:165–171
33. Frankfurt OS, Krishan A (2003) Apoptosis-based drug screening and detection of selective toxicity to cancer cells. Antican Drugs 14:555–561
34. Elsayed SA, Saad EA, Mostafa SI (2018) Development of new potential anticancer metal complexes derived from 2-hydrazinobenzothiazole. Mini Rev Med Chem. https://doi.org/10.2174/1389557518666181017143548
35. Feng Q, Liu Y, Huang J, Chen K, Huang J, Xiao K (2018) Uptake, distribution, clearance, and toxicity of iron oxide nanoparticles with different sizes and coatings. Sci Rep 8, Article number: 2082. https://doi.org/10.1038/s41598-018-19628-z
36. Vaja F, Guran C, Ficai D, Ficai A, Oprea O (2014) Cytotoxic effects of ZnO nanoparticles incorporated in mesoporous silica. UPB Sci Bull 76:55–66
37. Dickson MA, Schwartz GK (2009) Development of cell-cycle inhibitors for cancer therapy. Curr Oncol 16:36–43
38. Chen B, Yang J-Z, Wang L-F, Zhang Y-J, Lin X-J (2015) Ifosfamide-loaded poly (lactic-*co*-glycolic acid) PLGA-dextran polymeric nanoparticles to improve the antitumor efficacy in Osteosarcoma. BMC Cancer 15:752. https://doi.org/10.1186/s12885-015-1735-6
39. Mielcke TR, Muradás TC, Filippi-Chiela EC, Amaral MEA, Kist LW, Bogo MR et al (2017) Mechanisms underlying the antiproliferative effects of a series of quinoxaline-derived chalcones. Sci Rep 7:15850. https://doi.org/10.1038/s41598-017-16199-3
40. Singh SK, Lillard JW Jr, Singh R (2018) Reversal of drug resistance by planetary ball milled (PBM) nanoparticle loaded with resveratrol and docetaxel in prostate cancer. Cancer Lett 427:49–62. https://doi.org/10.1016/j.canlet.2018.04.017